Polyelectrolyte Brushes Grafted at the Air/Water Interface

Heiko Ahrens,[†] Stephan Förster,[‡] and Christiane A. Helm*[,†,§]

Institut für Physikalische Chemie, Johannes Gutenberg-Universität Mainz, Jakob-Welder Weg 11, 55099 Mainz, Germany, Max-Planck Institut für Kolloid- & Grenzflächenforschung, Kantstrasse 55, 14513 Teltow, Germany, and Fachrichtung Experimentalphysik, Universität des Saarlandes, Postfach 151150, 66041 Saarbrücken, Germany

Received June 27, 1997; Revised Manuscript Received September 23, 1997[⊗]

ABSTRACT: A new approach for the study of grafted polyelectrolytes is investigated: monolayers at the air/water interface of block copolymers consisting of a liquid hydrophobic and a polyelectrolyte block. The lateral interactions between the molecules is extremely long-ranged; a lateral pressure can be measured, while the grafting density is varied by a factor of 10. Furthermore, the isotherms show a phase transition. With specular X-ray reflectivity the segment density profile along the isotherm in the compressed phase is determined. The hydrophobic block shows features characteristic of a melt: constant electron density and a linear relationship between length and grafting density. In contrast, the length of the polyelectrolyte block amounts to 66% of the contour length and remains constant while the grafting density is varied by a factor 2. These features are typical for an osmotic brush phase.

Introduction

Despite many efforts, the conformation of a charged polymer chain in water is only partly understood.[1] Recently, polyelectrolytes anchored at an interface have attracted a lot of attention from the theoreticians,[2−4] not only because it is an extension of the now famous and classical problem of grafted polymers,[5,6] but also because it has been thought that, in this restricted geometry, the behavior of charged chains would be more easily understandable. Neutral anchored chains in a good solvent arrange themselves in a few phases, which can be distinguished experimentally and theoretically: at very low grafting densities isolated coils are found ("mushroom regime"), whereas at very high grafting densities the chains interact sterically and are therefore stretched ("brushes"). At intermediate grafting densities, an overlap regime is observed. Additionally to the entropic and elastic interactions found within and between uncharged chains, the polyelectrolyte conformation is influenced by the fraction of charged monomers, the concentration c_s of monovalent salt in solution, and the interaction between solvent and polymer segments. Therefore, an extremely rich phase behavior is predicted.[2,3]

We suggest a simple way to approach this problem experimentally. We investigate block copolymers consisting of a hydrophobic and a polyelectrolyte block at the air/water interface. Similar to smaller amphiphilic molecules on a Langmuir trough,[7,8] the block copolymers self-organize, the hydrophobic moiety is turned toward the air, and the hydrophilic one is immersed in water.[9,10] For the hydrophobic block, we chose poly(ethylethylene) (PEE), because the glass transition is below 0 °C.[11] Under these conditions, hydrophobic chains are expected to form a thin polymer melt of constant mass density.[12] At the air/water interface, the relevant parameters (nature of salt, salt concentration, pH, temperature) are easily accessible. With a Langmuir trough the grafting density of the polymer can be varied with a barrier while the lateral pressure is measured.

The onset of the lateral pressure increase and the slope of the isotherm indicate the range and strength of the lateral interaction of the polyelectrolyte chains. According to classical thermodynamics, abrupt slope changes of the pressure/area diagram are indicative of phase transitions. While the thermodynamic characterization is useful and necessary, the ultimate goal is a picture on a molecular scale. Therefore, we determine the electron-density profile of the anchored polyelectrolytes with X-ray reflectometry.[13,14] This method appears to be rather suitable, we will show that the length of the anchored chains as well as their detailed profile can be determined.

Materials and Methods

The chemical structure of the block copolymer PEE_{114}-$PSSH_{83}$ is shown in Figure 1. It was synthesized by a three-step procedure: (1) anionic block copolymerization of butadiene and subsequent addition of styrene delivers poly(1,2-butadiene-*block*-styrene). (2) Catalytic hydrogenation of the olefin residue and (3) application of the polystyrene sulfonation procedure lead after a subsequent ion exchange (Na^+ vs H^+) to the desired block copolymer.[15] The degree of sulfonation is 85%. It is dissolved in a solution of $CHCl_3$/CHOOH, (3:1) in a concentration of 1 mg/mL and spread on the aqueous solution. From the spread amount of block copolymer the grafting density is calculated. All measurements are performed at 20 °C.

A Langmuir trough (6 × 40 cm^2) was used for thermodynamic characterization. The barrier movement as well as the measurement of the lateral pressure are controlled and recorded by computer. Because the compression ratio of the trough is only 1:3, an isotherm is recorded starting from 0 mN/m, and the film is compressed as much as technically possible. Then the monolayer is expanded again, more block copolymer is spread, and the film is compressed until collapse. Good overlap is obtained by this stepwise recording (cf. Figure 2). The area calibration was reproducible within 8%.

For X-ray experiments we use a home-built setup[16] in a specular reflection geometry, incident and exit angles are identical ($q_i = q_f$), and the wave vector transfer corresponds to $Q_z = 4\pi/\lambda \sin\theta$. The light source is a standing Cu anode (λ = 1.54 Å, U = 40 kV, I = 55 mA) with a line focus, the beam is collimated by two slits (400 and 200 μm, respectively) before hitting the sample. The divergence of the reflected light is reduced by two additional slits (200 and 400 μm, respectively), a secondary monochromator reflects the light into a NaJ detector. Both the anode and detector sit on turntables, whose heights can be adjusted. The films were stable during reflec-

[†] Johannes Gutenberg-Universität Mainz.
[‡] Max-Planck Institut für Kolloid- & Grenzflächenforschung.
[§] Universität des Saarlandes.
[⊗] Abstract published in *Advance ACS Abstracts,* December 1, 1997.

S0024-9297(97)00949-2 CCC: $14.00

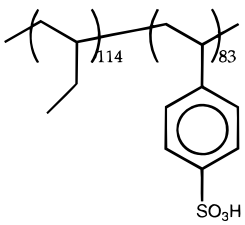

Figure 1. Structural formula of the block copolymer used.

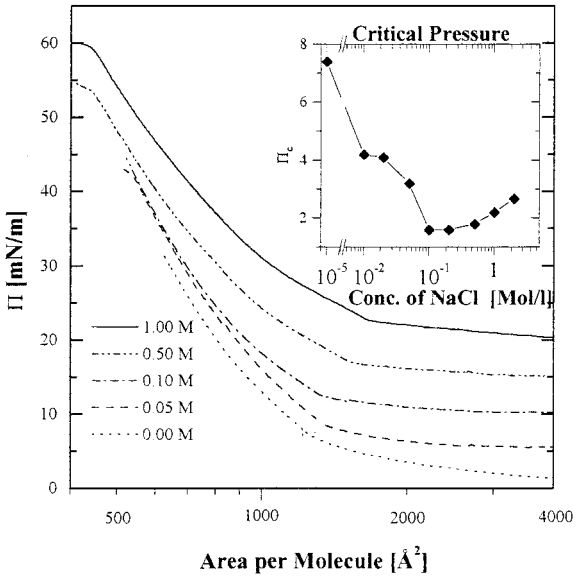

Figure 2. Pressure/area isotherms measured with different salt concentrations in solution. At about 1500 Å^2/molecule and a lateral pressure π_c, the change of slope in the isotherm indicates a phase transition. The dependence of π_c from the salt content in the subphase is shown in the inset. For clarity, each isotherm is displaced by 5 mN/m. Note the logarithm at the area axis.

tivity measurements, which took from 2 to 15 h. To avoid water evaporation and background scattering, the Langmuir trough is in a gastight enclosure filled with helium. The data are background-corrected. All experiments are repeated at least once with a newly prepared monolayer.

Specular reflection of X-rays provides information on the electron-density variation (scattering-density-length variation) perpendicular to the surface with Å resolution. For X-rays, the index of refraction depends only on the electron density ρ and various constants (the Thomson radius r_o)

$$n = 1 - \frac{r_o}{2\pi}\rho\lambda^2 \tag{1}$$

The reflectivity may be seen as the Fresnel reflectivity R_F of an infinitely sharp interface modulated by interference effects from the thin surface layer. The refractive index of the layer and substrate is only slightly less ($\approx 10^{-5}$) than 1. Therefore, dynamic effects (i.e., multiple scattering) or beam refraction contribute significantly to the reflectivity R only at small angles of incidence. Above about three critical angles the reflectivity can be described by the kinematic approximation[17]

$$\frac{R}{R_F} = \frac{1}{\rho_{sub}^2}\left|\int \rho'(z) e^{iQ_z z}\, dz\right|^2 \tag{2}$$

where ρ_{sub} is the electron density of the bulk phase ($\rho_{sub} = 0.334$ e$^-$/Å^3 for clean water), $\rho'(z)$ is the gradient of the electron density along the surface normal and Q_z is the wave vector transfer normal to the surface. Equation 2 gives an intuitive understanding, yet to avoid the approximations close to the critical angle, we work with the exact Fresnel formalism.[18] Due to the loss of phase information in conventional X-ray reflectivity experiments, the data analysis is generally based on finding proper electron density functions whose reflectivity properties match best the observed data.

Results

Figure 2 shows the isotherms of the block copolymer on clean water and on NaCl solutions. The principle features of the isotherms are always the same: at large areas per molecule (≈4500 Å^2/molecule) the lateral pressure starts to increase, at a lateral pressure π_c (A_c ≈ 1500 Å^2/molecule) a change of slope occurs, and after a fast pressure rise the film collapses (400−600 Å^2/molecule). On compression/expansion cycles, there is only a slight hysteresis, indicating the monolayer is basically in thermodynamic equilibrium. The phase transition pressure π_c depends nonmonotonically on the concentration of the NaCl solution (cf. inset of Figure 2): it decreases with increasing salt concentration until 0.1 M; then it slowly rises again. As long as π_c falls, A_c is constant, yet at high salt concentrations, both π_c and A_c increase. The higher the salt concentration, the more the film can be compressed before it collapses.

The decrease in the transition pressure π_c from 7.5 to 2 mN/m on increase of the ionic strength from clean water ($c_s = 5 \times 10^{-5}$ M) to $c_s = 1$ M is of the same order of magnitude as found with a phospholipid monolayer that can be described as a homogeneously charged planar surface.[19−21] Yet the nonmonotonic behavior cannot be explained to be due to a homogeneously charged surface.

Unusual for a Langmuir monolayer is the large compression ratio of the isotherm, a lateral pressure can be measured while the area/molecule is varied by a factor of ≈10 (15 for clean water). A factor of 2 is typical for both short-chain amphiphiles[7] as well as for fluid hydrophobic polymer chains anchored by a small hydrophilic group.[12,22] Indeed, for $N \approx 100$ monomers in the hydrophobic chain the first measurable pressure increase due to repulsive entropic interactions is expected to occur at molecular areas of 200−300 Å^2/molecule.[22] At such high grafting densities the PEE_{114}-PSS_{83} monolayer is already collapsed. Therefore, the PEE chains do not contribute to the isotherms observed.

In Figure 3 normalized X-ray reflectivity curves of the block copolymer on clean water are shown, measured at different points in the isotherm, as indicated in the inset. Curve a of Figure 3 is measured just at the pressure π_c. The narrow maximum at small Q_z is small, making the analysis extremely difficult for more expanded films. In principle, the curves are similar: At low Q_z there is one narrow maximum followed by a shallow minimum. At high Q_z one broad minimum occurs. On monolayer compression, the broad minimum shifts to lower Q_z; i.e., the film thickens. In contrast, the position of the narrow maximum at small Q_z remains constant within the resolution, yet its height increases from $R/R_F \approx 1.3$ (curve a) to $R/R_F \approx 1.6$, indicating a constant thickness accompanied by an increase in contrast. If the monolayer is assumed to consist of different homogeneous slabs, we can distinguish two different slabs, whose thickness is estimated according to

$$d = \frac{2\pi}{Q_{z,min}} \tag{3}$$

Then, the two slabs in curve a of Figure 3 measure 140 and 19 Å; in curve f these values are changed to

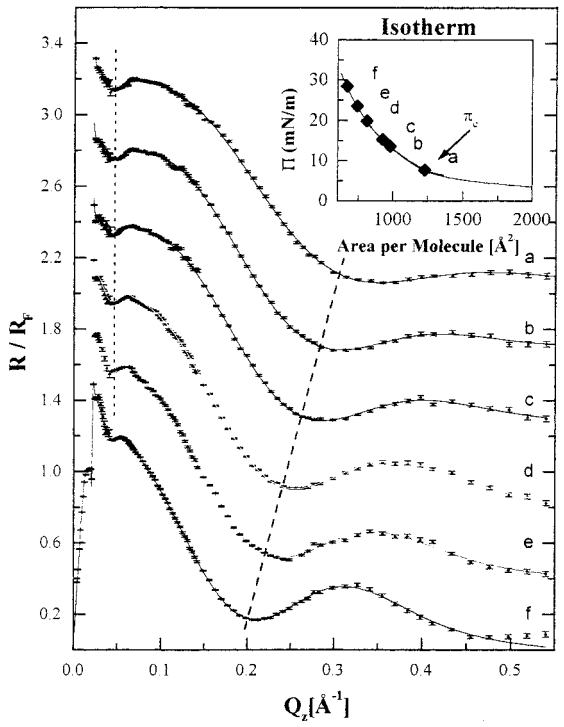

Figure 3. Normalized X-ray reflectivity measurements of the block copolymer $PEE_{83}PSS_{114}$ on a clean water subphase taken along the compressed phase, as indicated in the inset. The full lines are the simulated curves, from which the electron-density profile is deduced. For clarity, each reflectivity curve is displaced by 0.4. Curve f shows the complete reflectivity curve starting at angles below the critical momentum transfer of water, $Q_z = 0.21$ Å^{-1}, and the accompanying intensity enhancement together with the footprint. To concentrate on the monolayer, the reflectivity below the critical angle is not shown for the other curves.

137 and 38 Å, respectively. Due to interference effects, these numbers are subject to large errors, yet they describe the trends correctly. We may identify the thick slab with the polyelectrolyte block of almost constant thickness and the thin slab with a thickening hydrophobic block. (Detailed analysis will show that the broad minimum is caused by two slabs: the thickening hydrophobic slab and a flat PSS monolayer strongly attracted to the PEE.) Since only the first order of the narrow maximum is observed, the thick slab has to exhibit one extremely rough interface, the polyelectrolyte/water interface.

Due to the loss of phase information in conventional X-ray crystallography, the data analysis is generally based on finding proper electron density functions whose reflectivity properties retrospectively best match the observed reflectivity data. To obtain the optimum interfacial electron-density variation we used two different strategies.

(i) The layer is subdivided into slabs ("box model").[13,14] Each box is parameterized by a length and an electron density. The transition between adjacent boxes is smoothed. Proper smearing parameters describe the interfacial roughness. The parameters are determined by a least squares method. Box models are convenient because they can easily be applied to eq 2 and individual boxes may be identified with certain structural properties (e.g., representing aliphatic chains, head groups, etc.). For more complex electron-density profiles, however, many boxes are necessary to suitably describe the experimental data. This necessitates the determination of more adjustable parameters than one can unambiguously deduce from the reflectivity data, and various sets of parameters may result in the same electron-density profile within the experimental errors.[16,23] Yet, if different sets of parameters yield within error margins the same (optimum) model curve, the best fit parameters are not independent of each other and the errors of the fitted parameters are correlated. Therefore, a dependency analysis was performed.[18]

(ii) The electron-density profile is determined with a method that, in most cases, does not rely on *a priori* assumptions on the shape of the electron-density profile.[24,25] From the experimentally observed reflectivity curve the corresponding profile correlation function is estimated via indirect Fourier transformation. For this profile correlation function the matching scattering-length-density profile is then derived by square-root deconvolution. Both the correlation function and the density profile are expressed in terms of a linear combination of a set of suitable basic functions, whose coefficients are determined by least squares techniques. With this method, the number of basis functions, and thus, of free parameters, can be optimized (minimized) by a smoothness criterion for the correlation functions; thus, *a priori* assumptions on the electron-density profile can be avoided in most cases.

Our interpretation of the reflectivity data was considered satisfactory when the electron-density profile features resulting from the two different modeling processes were equivalent.

The monolayer is described as consisting of four different slabs, slab PEE1 is attributed to the hydrophobic block. The electron-density profile of the polyelectrolyte brush is parametrized by three slabs PSS1, PSS2, and PSS3. Two interfacial roughnesses are used, σ_2 for the interfaces adjacent to the PSS3 slab, σ_1 for all other interfaces (cf. Table 1). These are enough parameters to obtain good fits (cf. Figure 3).

The electron density of bulk PEE is 0.2963 e$^-$/Å^3 (deduced from the volume density of 0.8694 g/cm^3 [11]), which is somewhat higher than the experimentally determined value of $\rho_{PEE,average} = 0.281 \pm 0.006$ e$^-$/Å^3. Due to the constant mass density, the thickness of a melt is expected to increase linearly with the lateral grafting density $1/A$, as is indeed the case (cf. Figure 4). Yet, if we calculate the number of electrons in the hydrophobic slab ($N_{PEE} = \rho_{PEE} d_{PEE} A$), we find it is constant, as expected, but 30% lower than the bulk volume data, which is difficult to understand. Still, we can describe the PEE chains as a nanometer-thick hydrophobic melt. Furthermore, the PEE chains do not dewet as they do when anchored with a monomeric head group[12,22] and stretch to form a homogeneous film.

To describe the polyelectrolyte block, more parameters are necessary (cf. Table 1). The calculated electron-density profiles for the grafting densities investigated are given in Figure 5a. The contrast obtained is due to the fact that the electron density of a dehydrated PSS segment is higher than the one of water; in fact a PSS segment has 90 electrons (taking into account the 85% sulfonation) and a volume of 200 Å^3 (estimated from space filling models and ref 26). This yields an electron density of 0.46 e$^-$/Å^3.

A very reliable parameter, independent of the simulation strategy, is the overall thickness $d_{PSS1} + d_{PSS2} + d_{PSS3}$ (137 ± 1.6 Å), 66% of the contour length (207 Å) (cf. Figure 5b). Considering the original reflectivity data in Figure 3, this is no surprise, since the position of the narrow maximum is constant.

Table 1. Electron Densities (Relative to Water) and Lengths Attributed to the Slabs Used in Fitting the Data to the Model Described in the Text[a]

		PEE		PSS1		
area (Å$^{2)}$	π (mN/m)	length (Å)	rel el density	length (Å)	rel el density	roughness σ_1 (Å)
12.3E2	7.7	8.4	0.79	11.7	1.17	2.5
9.80E2	13.6	9.6	0.81	12.9	1.16	2.6
9.26E2	15.3	10.6	0.82	12.7	1.16	2.8
8.13E2	19.9	12.9	0.87	11.6	1.19	3.3
7.40E2	23.6	13.9	0.87	11.9	1.19	3.4
6.66E2	28.5	15.9	0.88	13.2	1.18	3.4
		PSS2		PSS3		
area (Å$^{2)}$	π (mN/m)	length (Å)	rel el density	length (Å)	rel el density	roughness σ_2 (Å)
12.3E2	7.7	0.4	1.07	126.1	1.03	32.2
9.80E2	13.6	3.5	1.06	119.6	1.02	33.1
9.26E2	15.3	15.6	1.05	102.4	1.02	28.7
8.13E2	19.9	0.1	1.08	124.9	1.03	35.2
7.40E2	23.6	0.1	1.09	126.4	1.03	32.7
6.66E2	28.5	0	1.11	128.2	1.04	36.3

		V (Å^3)				N_{Elec}				
area (Å^2)	π (mN/m)	PEE	PSS1	PSS2	PSS3	PEE	PSS1	PSS2	PSS3	total length H (Å)
12.3E2	7.7	1.04E4	1.45E4	4.98E2	1.55E5	2.76E3	5.66E3	1.79E2	5.34E4	138.5
9.80E2	13.6	9.45E3	1.27E4	3.50E3	1.17E5	2.58E3	4.96E3	1.24E3	4.03E4	136.1
9.26E2	15.3	9.83E3	1.18E4	1.45E4	9.48E4	2.72E3	4.60E3	5.10E3	3.24E4	130.8
8.13E2	19.9	1.05E4	9.43E3	1.24E2	1.01E5	3.09E3	3.77E3	4.47E1	3.52E4	136.6
7.40E2	23.6	1.03E4	8.84E3	1.15E2	9.35E4	3.02E3	3.52E3	4.21E1	3.24E4	138.5
6.66E2	28.5	1.06E4	8.83E3	0	8.53E4	3.16E3	3.50E3	0	2.98E4	141.4

[a] $V = Ad$ is the volume per slab, and $N_{Elec} = V\rho_{Elec}$, its numbers of electrons.

All the electron-density profiles in Figure 5a exhibit a maximum close to the anchoring interface, which is parametrized by the PSS1 slab. Actually, the electron density $\rho_{PSS1,average} = 0.392 \pm 0.002$ e$^-$/Å^3 and the length of the PSS1 slab, $d_{PSS1,average} = 12.3 \pm 0.3$ Å are parameters that remain constant while the anchoring density is varied by a factor of 2. From molecular considerations, we found that the cross-section of a stretched PSS chain with atactic (random) side group distribution exhibits 3-fold symmetry. The diameter of the theoretical chain is 13.1−15.2 Å,[27] which corresponds to the thickness of the PSS1 slab. Apparently, the PSS chain is attracted to the PEE layer, and a 2-dimensional PSS coil lays beneath the PEE block. From the electron density ρ_{PSS1}, we can calculate the amount n of water molecules in this 2-dimensional PSS coil

$$\rho_{PSS1} = \frac{N_{el,PSS-monomer} + nN_{el,H_2O}}{V_{PSS-monomer} + nV_{H_2O}} = \frac{90 + n10}{200 + n30} \quad (4)$$

This calculation yields six water molecules per PSS monomer. To form a close-packed monolayer, at the phase transition ($A_c = 1260$ Å^2) on average 38 monomers from the PSS chain are attracted to the PEE layer. At the highest grafting density ($A = 670$ Å^2), only 20 monomers per chain are confined to the monolayer. It is interesting to compare these results with adsorption experiments of PSS onto hydrophobic latex particles,[28] where a "monolayer" PSS adsorbed, stabilizing the polystyrene latices in aqueous solutions.

Beneath this 2-dimensional PSS coil, the electron density decreases monotonically. In terms of X-ray reflectivity measurements we find the PSS2 slab necessary to smooth the transition between the peak in the electron density described by the PSS1 slab and the slow decay in electron density of the brush described by the PSS3 slab. The two parameters describing the PSS2 slab (density and thickness) depend strongly on each other; therefore we shall refrain from discussion. We tried to find other functions to describe the electron-density profile less ambiguously (Gaussian, parabolic), but we did not yet succeed.

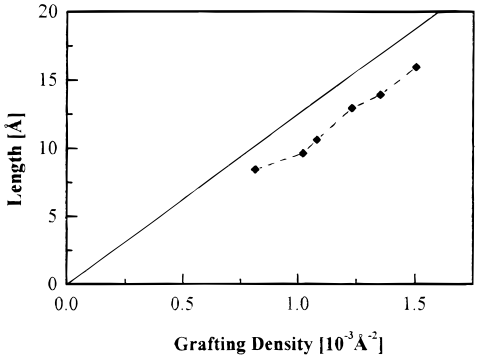

Figure 4. Thickness of the hydrophobic PEE block anchor as deduced from the simulations of the electron-density profile (d_{PEE}; cf. Table 1). The straight line is calculated under the assumption that the hydrophobic block exhibits the same mass density as the bulk phase.

The water-adjacent PSS3 slab is more interesting. It describes the long water-immersed part of the polyelectrolyte chains. On compression, the electron density is increasing; i.e., water is removed between the chains.

The roughness of the PSS3 interfaces is extremely high, $\sigma_2 = 33$ Å; with this roughness the slow decay of the electron density is described, as is the asymmetrical distribution of the chains. The other interfaces are much less smeared, $\sigma_1 \approx 2.5-3.5$ Å. The low roughness σ_1 is typical for the air/water interface and is usually explained in the framework of the theory of capillary waves.[29,30]

We changed the parametrization in the way that the overall length of the brush, $H = d_{PSS1} + d_{PSS2} + d_{PSS3}$, was an independent parameter (the slabs being characterized now by d_{PSS1}, $H - d_{PSS1} - d_{PSS3}$, and d_{PSS3})

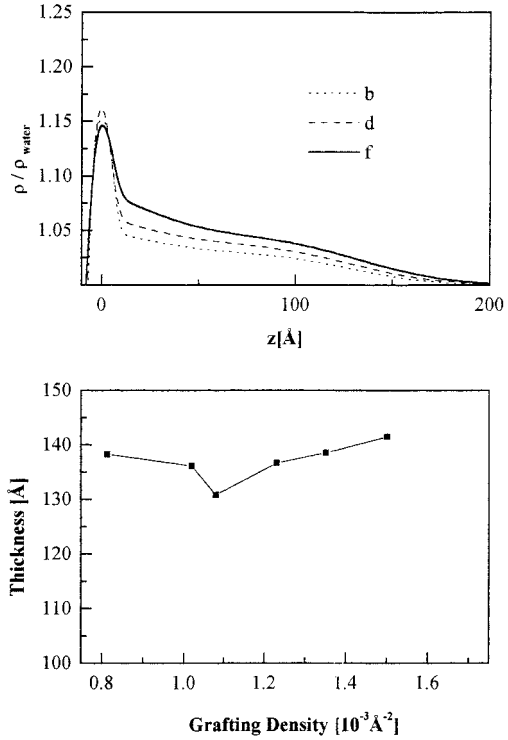

Figure 5. (a) The electron-density profiles of the polyelectrolyte block for the area per molecule as indicated. There is a thin slab of increased electron density, presumably due to a PEE/PSS attraction, which remains constant. The thickness of the block is constant, whereas the electron density of the main part increases (i.e., water between the polyelectrolytes is removed). (b) The thickness of the polyelectrolyte part of the monolayer ($H = d_{PSS1} + d_{PSS2} + d_{PSS3}$; cf. Table 1) as function of the area/molecule is constant in the compressed phase, an unusual feature typical for an osmotic brush.

and found that the error of the brush thickness H supplied by the Marquardt−Levenberg fit routine and also in the dependency analysis was lower than for any of the thicknesses describing the individual slabs.[18]

Discussion

From the combination of isotherms and the detailed analysis of reflectivity measurements of block copolymer monolayers, the following picture emerges: If the monolayer is compressed beyond a phase transition, the hydrophobic chains behave like a nanometer-thick hydrophobic melt (even though of low density with missing electrons). The polyelectrolyte part of the monolayer is much more stretched (137 Å); it amounts to 66% of the contour length (208 Å). The thickness of the polyelectrolyte moiety is constant, when the anchoring density is varied by a factor of 2.

Directly beneath the hydrophobic anchors the electron density is highest; obviously, there is a strong attraction between the PSS and the PEE, presumably due to the hydrophobic nature of the PSS backbone. Indeed, a PSS monolayer is found, on average, hydrated by six water molecules. Then, the polyelectrolyte chain appears to be mainly oriented perpendicular to the surface. On compression, the electron density of the long water-immersed part increases, due both to water expulsion and to PSS monomers being removed from the PEE-adjacent 2-dimensional PSS chain.

Considering the theoretical work, a thickness independent of the grafting density is found for noninteracting polyelectrolytes at very low grafting densities (oriented sticks) and also for the osmotic brush.[3]

The "osmotic brush" phase is expected for grafting areas below an overlap threshold, which is defined according to $A \cong H_o^2$ with H_o as the length of an isolated polyelectrolyte chain grafted to a surface. This value is not known, so we have to estimate: assuming a Kuhn length of $l_k = 100$ Å (an estimate on the low side), we find for the unperturbed coil $R_0^2 = Nal_k = 83 \cdot 2.5$ Å$\cdot 100$ Å $= 20\,750$ Å^2 (with the contour length $Na = 207.5$ Å). Presumably, this is the upper limit for the overlap threshold. The lower limit is the radius of gyration $R_g \approx 40$ Å of uncharged polystyrene with $N = 83$ ($R_0 = \sqrt{6}R_g$). This leads to a molecular area of $R^2 = 1600$ Å^2. The data shown in Figure 3 were measured in the regime of $A < 1200$ Å$^2 < R^2$, obviously below the lower limit of the overlap threshold.

In the case of the osmotic brush, all counterions are located inside the brush and form a homogeneous counterion cloud. The brush becomes electroneutral as a whole. Thus, the counterion density in the totally dissociated brush amounts to Q/AH, with H as the brush length and Q the total charge per chain. Thus, the stretching electrostatic force f_{el} is determined by the osmotic pressure

$$f_{el}/T \cong Q/H \tag{5}$$

which is counteracted by the elastic force f_{conf} (here given for a Θ-solvent)

$$f_{conf}/T \cong H/a^2N \tag{6}$$

($a \approx 2.5$ Å is the length per monomer unit, N is the amount of monomers per chain). The force balance yields

$$H \cong a(QN)^{1/2} \tag{7}$$

Equation 7 describes an unusual feature of the osmotic brush phase, a brush thickness independent of the grafting density. This feature is confirmed in the experiments presented here, yet the experimentally determined thickness is higher than theoretically predicted, 137 Å. The neglected effects are Manning condensation, which would reduce the charge per chain, and the sterical constraints the chains experience due to the attraction of the PEE. These additional conformational changes do not appear to change the overall length, which is determined by the counterion gas. Therefore, we may conclude that the chains are indeed in the osmotic brush phase (cf. Figure 6).

In the future, when we work with increased ion concentration in the solution to shield the intrachain electrostatic interactions, we expect to see a shortening of the brush. If elastic interactions are of the same order of magnitude as the electrostatic, we expect to see an increase in chain thickness on compression. Also, we hope to be able to investigate the expanded monolayer below the phase transition. Furthermore, variation in the chain length of the respective polymer block will provide further insight into the chain stretching.

Conclusions and Implications

We demonstrate that block copolymers consisting of a fluid hydrophobic and a polyelectrolyte moiety form stable monolayers at the air/water interface. The molecules exhibit an extremely long-range lateral repulsion of presumably mainly electrostatic origin. With X-ray reflectivity the electron-density profile of the

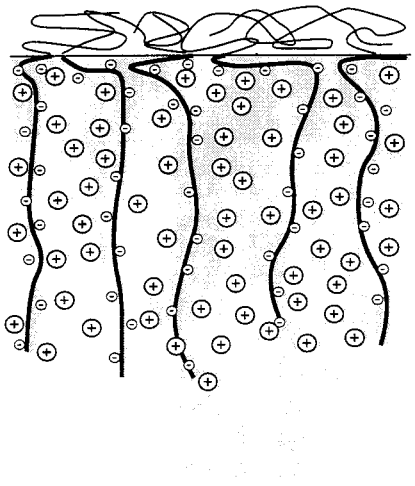

Figure 6. Schematics of the monolayer in the osmotic brush phase.

compressed phase is probed. The hydrophobic anchor can be described as a nanometer-thick hydrophobic melt. The polyelectrolyte moiety is extremely stretched; the thickness (66% of the contour length) remains constant while the anchoring density is varied by a factor of 2. Beneath the hydrophobic anchor a PSS monolayer is formed with a hydration of six water molecules per monomer. (This is a lot, the degree of hydration of PSS adsorbed onto a solid support is 3−4 water molecules.) This is indicative of a strong PEE−PSS attraction (presumably of hydrophobic nature), yet the interchain interactions do not influence the brush length, which is determined by the osmotic pressure of the counterion gas. The thermodynamic data indicate further an expanded phase, which is tentatively attributed to oriented sticks.

There are three main advantages to the use of block copolymers at the air−water interface as models for grafted polyelectrolytes: (i) In contrast to polyelectrolytes grafted onto a solid support,[31] the anchoring density can be varied in situ. (ii) To probe the segment density profile, a higher resolution (i.e., a higher wavevector transfer) is achieved with a home-built X-ray reflectometer[16] than with a neutron facility,[31] basically for flux reasons. (iii) In the future, the profile of the coions and counterions may be obtained. There are disadvantages, too: (i) the grafting density is limited by film collapse. (ii) We showed that contrast inversion is possible with high salt solution,[32] yet it cannot be as easily obtained as with neutrons. Thus, the approach proposed in this paper does yield results complementary to neutron reflection.

With model systems of this kind the behavior of polyelectrolyte chains may be studied extensively. Especially interesting are phase transitions. Questions on the dependence of stick thickness or brush thickness on solution conditions can be addressed. Fortunately, our most recent experiments indicate the contrast between anchored polyelectrolytes and solutions containing ions with a high atom number provide better contrast and better resolved electron-density profiles than the experiments shown here.

Acknowledgment. We acknowledge intense discussions with Helmuth Möhwald. J. Schmitt helped us with the theoretical data on the volume of a PSS monomer. We are grateful to the Deutsche Forschungsgemeinschaft for founding the Schwerpunkt Polyelektrolyte, which gave us the means to collaborate (He 1616/7-1,2; Fö 246/2-1). Furthermore, C.A.H. thanks Karl Fischer for discussions on organic chemistry and Manfred Schmidt for his hospitality.

References and Notes

(1) Förster, S.; Schmidt, M. Polyelectrolytes in Solution. In *Physical Properties of Polymers*; Wegner, G., Ed.; Springer Verlag: Berlin, Heidelberg, 1995; pp 51−133.
(2) Israëls, R.; Leermakers, F. A. M.; Fleers, G. J. *Macromolecules* **1994**, *27*, 2087−3093.
(3) Borisov, O. V.; Zhulina, E. B.; Birshtein, T. M. *Macromolecules* **1994**, *27*, 4795.
(4) Zhulina, E. B.; Birshtein, T. M.; Borisov, O. V. *Macromolecules* **1995**, *28*, 1491.
(5) Alexander, S. *J. Phys.* **1977**, *38*, 983.
(6) Gennes, P.-G. d. *Macromolecules* **1980**, *13*, 1069.
(7) Möhwald, H. *Rep. Prog. Phys.* **1993**, *56*, 653.
(8) Evans, F.; Wennerström, H. *The Colloidal Domain: Where Physics, Biology, and Technology Meet*; VCH: Weinheim, New York, 1994.
(9) Li, Z.; Zhao, M. W.; Quinn, J.; Rafailovich, M. H.; Sokolov, J.; Lennox, R. B.; Eisenberg, A.; Wu, X. Z.; Kim, M. W.; Sinha, S. K.; Tolan, M. *Langmuir* **1995**, *11*, 4785−4792.
(10) Kim, S.; Yu, H. *J. Phys. Chem.* **1992**, *96*, 4034.
(11) Rosedale, J. H. City, 1993.
(12) Baltes, H.; Schwendler, M.; Helm, C. A.; Heger, R.; Goedel, W. A. *Macromolecules*, in press.
(13) Helm, C. A.; Möhwald, H.; Kjaer, K.; Als-Nielsen, J. *Europhys. Lett.* **1987**, *4*, 697−703.
(14) Bosio, L.; Benattar, J. J.; Rieutord, F. *Rev. Phys. Appl.* **1987**, *22*, 775−778.
(15) Förster, S.; Hermsdorf, N.; Leube, W. **1998**.
(16) Baltes, H.; Schwendler, M.; Helm, C. A.; Möhwald, H. *J. Colloid Interface Sci.* **1996**, *178*, 135−143.
(17) Als-Nielsen, J. Solid and liquid surfaces studied by synchrotron x-ray diffraction. In *Structure and Dynamics of Surfaces*; Blanckenhagen, W. S. a. W., Ed.; Springer: New York, 1986.
(18) Asmussen, A.; Riegler, H. *J. Chem. Phys.* **1996**, *104*, 8159−8164.
(19) Helm, C. A.; Laxhuber, L. A.; Lösche, M.; Möhwald, H. *Colloid Polym. Sci.* **1986**, *264*, 46−55.
(20) Payens, T. *Phillips Res. Rep.* **1955**, *10*, 425.
(21) Marra, J. *Biophys. J.* **1986**, *50*, 815−825.
(22) Heger, R.; Goedel, W. A. *Macromolecules* **1996**, *29*, 8912.
(23) Tidswell, I. M.; Ocko, B. M.; Pershan, P. S.; Wasserman, S. R.; Whitesides, G. M.; Axe, J. D. *Phys. Rev. B* **1990**, *41*, 1111.
(24) Pederson, J. S. *J. Appl. Crystallogr.* **1992**, *25*, 129−145.
(25) Pederson, J. S.; Hamley, I. W. *J. Appl. Crystallogr.* **1994**, *27*, 36−49.
(26) Schmitt, J.; Grünewald, T.; Kjær, K.; Pershan, P.; Decher, G.; Lösche, M. *Macromolecules* **1993**, *26*, 7058−7063.
(27) Donath, E.; Walter, D.; Shilov, V. N.; Knippel, E.; Budde, A.; Lowack, K.; Helm, C. A.; Möhwald, H. *Langmuir* **1997**, *13*, 5294−5305.
(28) Müller, H.; Leube, W.; Tauer, K.; Förster, S.; Antonietti, M. *Macromolecules* **1997**, *30*, 2288.
(29) Schwartz, D. K.; Schlossman, M. L.; Kawamoto, E. H.; Kellogg, G. J.; Pershan, P. S. *Phys. Rev. A* **1990**, *41*, 5687−5690.
(30) Daillant, J.; Bosio, L.; Benattar, J. J.; Meunier, J. *Europhys. Lett.* **1989**, *8*, 453−458.
(31) Mir, Y.; Auroy, P.; Auvray, L. *Phys. Rev. Lett.* **1995**, *75*, 2863−2866.
(32) Ibn-Elhaj, M.; Riegler, H.; Möhwald, H.; Schwendler, M.; Helm, C. A.; *Phys. Rev. E* **1997**, *56*, 1844−1852.

MA970949E